Smart Structures and Systems, *Vol. 35, No. 3 (2025) 141-151*
https://doi.org/10.12989/sss.2025.35.3.141

Displacement response reconstruction method for bridge subjected to moving load based on IPSO-BiLSTM network

Wen-Yu He [1,2], Ao Gao [1], Yi-Fan Li [1] and Dong-Yang Hu*[3]

[1] *Hefei University of Technology, Hefei, Anhui Province, 230009, China*
[2] *Anhui Province Road and Bridge Inspection Engineering Research Center, Hefei, Anhui 230009, China*
[3] *Kunming Survey, Design and Research Institute Co., Ltd. of CREEC, Kunming 650200, China*

(*Received January 2, 2024, Revised March 1, 2025, Accepted March 3, 2025*)

Abstract. Bridge dynamic displacement reconstruction methods based on neural networks usually use single-input neural networks, and most of the hyperparameters are determined by experience, which seriously affect the reconstruction accuracy. In this paper, a reconstruction method for bridge displacement response induced by moving load is proposed by using a small number of sensors and a triple-input IPSO-BiLSTM network. Firstly, the input strain and acceleration data are normalized in advance for data fusion. Secondly, IPSO-BILSTM network model with three-time sequence responses as input is constructed, and IPSO algorithm is used to optimize the network hyperparameters. Finally, three-time sequence responses are input into the trained iterative particle swarm optimization (IPSO)-Bidirectional LSTM (IPSO-BiLSTM) neural network to reconstruct the bridge displacement response. The proposed IPSO-BiLSTM network realizes the data fusion of three-time sequence responses and automatically establishes the relationship between input response and output displacement. Numerical examples indicate that the reconstruction accuracy is sensitive to road roughness and measurement noise. Experimental studies reveal that the reconstruction accuracy is insensitive to vehicle velocity and weigh.

Keywords: bridge displacement reconstruction; hyperparameters optimization; IPSO-BiLSTM Network; moving load

1. Introduction

Bridge displacement response induced by moving load is an important index to evaluate the bridge safety (Hester *et al*. 2017). The sensing technology for directly measuring dynamic displacement mainly includes linear variable differential transformer (LVDT) (Joshi and Harle 2017), Laser Doppler Vibrometer (LDV) (Nassif *et al*. 2005), interferometric radar, Real Time Dynamic Global Navigation Satellite System (RTK-GNSS), and computer vision-based methods (Ni *et al*. 2019, Martini *et al*. 2022). However, there are several concerns for the above-mentioned direct methods, such as additional supports under the bridge are required for LVDT (Moreu *et al*. 2015), LDV and interferometric radar are expensive and inconvenient for long-term monitoring, the accuracy and sampling rate of RTK-GNSS are low, the accuracy of vision-based system is greatly affected by illumination and weather thought it can track the initial condition of dynamic displacement response is usually acceleration or strain, have attracted much attention. As the physical quantities related to displacement, such as unknown, the displacement reconstruction method based on double methods for reconstructing displacement by displacement of multiple points. In view of this, the indirect measuring integration of acceleration suffers error caused by numerical integration in discrete time domain. Besides, the error will be amplified by continuous integration, which results in low-frequency drift on the reconstructed displacement (Stiros 2008). Though techniques have been developed for suppressing low-frequency drift, they often cannot distinguish the difference between actual structural response and noise in the same low-frequency band (Lee *et al*. 2010). Modal superposition or curvature fitting techniques are normally used for most of the strain-based displacement estimation methods (Cheng *et al*. 2018). Wang *et al*. (2014) used the cross-correlation function of dynamic strain data to identify strain mode shape of simply supported beam and then estimated dynamic displacement according to the principle of modal mapping and modal superposition. Vurpillot *et al*. (1998) obtained the curvature function of the cross-section from strain response and then estimated vertical displacement of bridge by integrating the curvature function twice. Strain-based methods can reconstruct the low-frequency part of displacement, but the reconstruction accuracy decreases in the high-frequency part due to the influence of measurement noise. As the bridge displacement induced by moving load includes high-frequency vibration displacement and low-frequency pseudo-static displacement, obvious limitations appear when using indirect method of acceleration or strain alone to reconstruct displacement. Therefore, data fusion of different responses would be a natural choice (Duan *et al*. 2022, Hassani *et al*. 2023, Ma *et al*. 2021, Smyth and Wu 2007). Data fusion methods use a variety of sensors or data sources to estimate more accurate bridge displacement, which can be mainly

*Corresponding author, Master, Senior Engineer,
E-mail: hudyztey@163.com

ISSN: 1738-1584 (Print), 1738-1991 (Online)

classified into three categories:

(1) Combination of direct and indirect methods. As GPS usually performs better at low-frequency band, while accelerometers perform better at high frequency band, Kogan *et al*. (2008) estimated the bridge dynamic displacement by utilizing displacement and acceleration response measured by GPS and accelerometers, respectively. Kim and Sohn (2017) fused velocity measured by laser Doppler vibrometer and displacement measured by lidar for displacement reconstruction. However, mixing multiple measurement methods cannot completely overcome their own defects.

(2) Combination of two indirect methods. Park *et al*. (2013) proposed an indirect displacement estimation approach by fusing acceleration and strain data based on Kalman filter and least squares method. However, inaccurate scaling factors used for strain-displacement transformation usually reduced the estimation accuracy. Ma *et al*. (2021) presented a displacement estimation technique based on finite impulse response filter in which a scale factor was introduced to suppress integral drift and noise interference, but its effectiveness depended on the accuracy of scale factor.

(3) Machine learning algorithms such as neural networks can establish the relationship between input and output data. Moon *et al*. (2019) used multi-layer feed-forward neural networks, and Wang *et al*. (2022) developed an LSTM-based fusion method to estimate the bridge dynamic displacement. However, most existing neural network-based methods rely on single-input architectures and manually selected hyperparameters, which significantly limit their reconstruction accuracy. These limitations stem from the inability of single-input networks to effectively fuse multi-source dynamic responses and the lack of systematic optimization for critical hyperparameters.

To overcome the above-mentioned limitations, this study proposes a reconstruction method for bridge displacement response induced by moving load based on iterative particle swarm optimization (IPSO)-Bi directional LSTM (IPSO-BiLSTM) neural network. The main objectives are: (1) achieve high-precision data fusion of multi-source dynamic responses; (2) automatically optimize network hyper-parameters using the IPSO algorithm, eliminating reliance on empirical selection; and (3) enhance the robustness against measurement noise and varying load conditions. The remaining sections of this study are organized as follows. Section 2 outlines the basic theory of the proposed method. Section 3 provides a detailed implementation procedure. Section 4 presents the effectiveness of the proposed method according to the outcomes of numerical study. Section 5 discusses the robustness of proposed method. Section 6 demonstrates the effectiveness of the proposed method in experimental verification. Section 7 concludes the study.

2. Basic theory

2.1 Network model construction

The neural network model is used to describe the relationship between the measured strain and acceleration response (input) and displacement response (output). Generally, the output of a moment is related to the information of past and subsequent moments simultaneously. Therefore, this paper adopts a BiLSTM network including forward and backward LSTM neural networks. The BiLSTM network expanded according to time is shown in Fig. 1, and the hidden layer state h_t at time t is

$$h_t{}^1 = f(U^1 h_{t-1}{}^1 + W^1 x_t + b^1) \tag{1}$$

$$h_t{}^2 = f(U^2 h_{t-1}{}^2 + W^2 x_t + b^2) \tag{2}$$

$$h_t = h_t{}^1 \oplus h_t{}^2 \tag{3}$$

where $\oplus$ is the vector splicing operation.

The displacement response of an actual bridge at target point is related to the response of other points. As a single-input neural network, BiLSTM network still has shortcomings in displacement reconstruction. To address this problem, several BiLSTM network layers are added to input the temporal responses of other points, and a multi-input BiLSTM network is constructed accordingly. Then, according to Eq. (3), the hidden layer states of all BiLSTM network layers are spliced together as the final hidden layer state h_t. Typical dual-input BiLSTM network is presented in Fig. 2 as an example.

The bridge dynamic displacement induced by moving load includes vibration displacement caused by inertial force and pseudo-static displacement caused by gravity. If only the acceleration response is used, the reconstruction

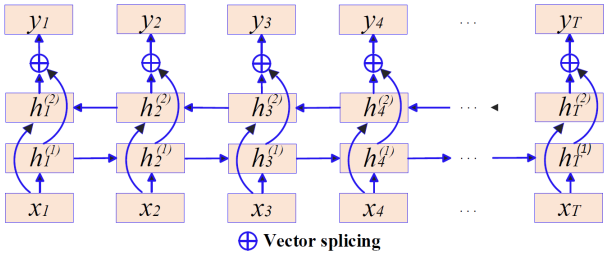

Fig. 1 BiLSTM expanded according to time

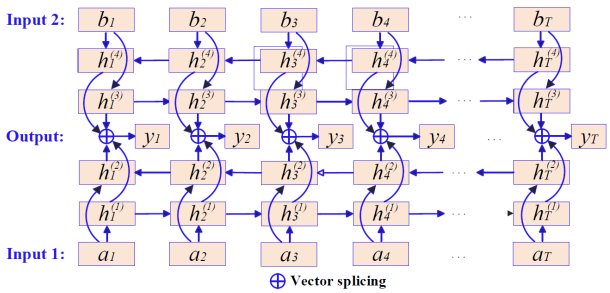

Fig. 2 Dual-input BiLSTM network

$$\omega = \begin{cases} \omega_{\min} - \dfrac{(\omega_{\max} - \omega_{\min})\left(f^i(t) - f_{\min}(t)\right)}{f_{avg}(t) - f_{\min}(t)}, & f^i(t) \le f_{avg}(t) \\ \omega_{\max}, & f^i(t) > f_{avg}(t) \end{cases} \tag{6}$$

accuracy will be affected by low-frequency noise. On the contrary, the reconstruction accuracy of high-frequency components is low if only the strain response is used. Therefore, the strain response of the symmetric points on the left and right sides close to the target point and the acceleration response at the target point are taken as inputs to construct the BiLSTM network in this paper.

2.2 Network model optimization

The main difficulty in neural network training is finding the global optimal solution, so the network model needs to be optimized. This section mainly introduces hyperparameter optimization, loss function and optimization algorithm involved in network model optimization.

2.2.1 Hyperparameter optimization

Hyperparameters significantly influence the network performance. Network structure including the number of hidden layers, the number of neurons in each layer, and optimization parameters. Training period and learning rate batch size are typical hyperparameters. Particle swarm optimization algorithm is widely used in the field of optimization. However, it suffers premature convergence to local optimum, slow convergence speed at the later stage of iteration and low search accuracy. In view of this, this paper utilizes improved particle swarm optimization (IPSO) to optimize network hyperparameters, including the number of hidden layers, the number of neurons in the hidden layer, the training period, and the learning rate.

Assuming that the particle swarm size is N, the current number of iterations is t, the position of the i^{th}particle is $x_i(t)$, and the velocity of the i^{th}particle is $v_i(t)$, the historical optimal positions of all particles in the entire particle swarm are $gbest(t)$, and the historical optimal positions of the i^{th} particle is $pbest_i(t)$. The velocity and position of the particle are updated according to Eq. (4) and (5).

$$\begin{aligned} v_i(t+1) = \omega v_i(t) t_1 r_1\left(pbest_i(t) - x_i(t)\right) \\ + t_2 r_2\left(gbest(t) - x_i(t)\right) \end{aligned} \tag{4}$$

$$x_i(t+1) = x_i(t) + v_i(t+1) \tag{5}$$

where r_1 and r_2 are uniform random numbers distributed in [0, 1]; ω is the inertia weight; t_1 and t_2 are individual learning factor and social learning factor, respectively.

The optimization performance of PSO depends on the inertia weight and learning factor. IPSO adopts adaptive inertial weight and adaptive learning factor, which improves the optimization accuracy of the algorithm on the premise of ensuring efficiency. Inertial weight is a parameter to balance global and local search capabilities in PSO, and IPSO adopts the adaptive inertial weight as in Eq. (6)

where $\omega_{\min}$ and $\omega_{\max}$ represent the minimum and maximum values of ω, respectively; $f^i(t)$ represents the current fitness value of the i^{th} particle at the i^{th} iteration; $f_{\text{avg}}(t)$ and $f_{\min}(t)$ are the average and minimum fitness values of all particles at the i^{th} iteration, respectively.

Individual learning factor t_1 and social learning factor t_2 determine the influence of particle individual and population on particle trajectory, respectively, which reflect the information exchange between particle swarms. IPSO algorithm adopts the adaptive learning factor, which can effectively control the velocity of particles and achieve the balance between global search and local search. The calculations of individual learning factor t_1 and social learning factor t_2 are shown in Eqs. (7) and (8).

$$t_1 = 0.5 + 2e^{[-(4t/T)^2]} \tag{7}$$

$$t_2 = 2.2 - 2e^{[-(4t/T)^2]} \tag{8}$$

where T is the total number of iterations.

2.2.2 Loss function

Loss function is used to evaluate the prediction results of the network model, and is important for adjusting parameters of neural network. The loss functions in the regression model include mean square error (MSE), mean absolute error (MAE) and smooth mean absolute error (HuberLoss), which are specific as

$$MSE = \frac{1}{m}\sum_{i=1}^{m}\left(y_i - f(x_i)\right)^2 \tag{9}$$

$$MAE = \frac{1}{m}\sum_{i=1}^{m}|y_i - f(x_i)| \tag{10}$$

$$L_\delta(y_i) = \begin{cases} \dfrac{1}{2}\left(y_i - f(x_i)\right)^2, & |y_i - f(x_i)| \le \delta \\ \delta|y_i - f(x_i)| - \dfrac{1}{2}\delta^2, & |y_i - f(x_i)| > \delta \end{cases} \tag{11}$$

For MSE, when the difference between y_i and $f(x_i)$ is larger than 1, the error will increase, and MSE will give larger penalty, and vice versa. Therefore, if there are outliers in the sample, MSE will give the outliers a higher weight, which will affect the prediction effect of other normal points and ultimately lead to the reduction of the overall performance of the model. On the contrary, MAE calculates the absolute value of the difference between y_i and $f(x_i)$, so the outliers are punished to the same degree and occupy the same weight. Compared with MSE, MAE is less sensitive to outliers and more inclusive. HuberLoss is a synthesis of MSE and MAE which reduces the sensitivity to outliers and is derivable everywhere. The hyperparameter δ determines the emphasis of HuberLoss on MSE and MAE.

In this paper, HuberLoss is used as the loss function.

2.2.3 Optimization algorithm

Optimization algorithms for training neural networks can be divided into two categories: (1) adjusting the learning rate to make the optimization more stable; (2) correcting gradient estimation to optimize training speed. The RMSprop algorithm and the momentum method are commonly used for learning rate adjustment and gradient estimation correction, respectively. Adam algorithm is a combination of RMS prop algorithm and momentum method (Kumar *et al*. 2022), which takes momentum as the direction of update parameter, and the learning rate is adaptively adjusted. In this paper, Adam algorithm is used to search model parameters of IPSO-BiLSTM network by gradient descent, and then the error back propagation of the network is carried out to update the parameters of the network model according to the loss value.

2.3 Data preprocessing

As the numerical values of different types of bridge responses are quite different, the collected response data is normalized by quantifying each feature of the sample into a unified interval and eliminating the correlation between each feature. The value range of strain and displacement data is normalized to [0, 1] by Eq. (12), and the value range of acceleration data is normalized to [-1, 1] by Eq. (13).

$$x_n^{'} = \frac{x_n - \min(\{x_n\}_{n=1}^N)}{\max(\{x_n\}_{n=1}^N) - \min(\{x_n\}_{n=1}^N)} \tag{12}$$

$$x_n^{'} = \frac{2\left(x_n - \min(\{x_n\}_{n=1}^N)\right)}{\max(\{x_n\}_{n=1}^N) - \min(\{x_n\}_{n=1}^N)} - 1 \tag{13}$$

where $\{x_n\}_{n=1}^N$ is a set containing N samples; $x_n^{'}$ is the value normalized for the original input at the time t; $max(\{x_n\}_{n=1}^N)$ and $min(\{x_n\}_{n=1}^N)$ are the maximum and minimum values of the set $\{x_n\}_{n=1}^N$, respectively.

The output data can be obtained and de-normalized through the preprocessed input data and the trained IPSO-BiLSTM network, and finally the dynamic displacement can be reconstructed.

3. Displacement response reconstruction method

The procedures of the bridge displacement response reconstruction are shown in Fig. 3, specific as:

Step 1: Data preprocessing. The collected bridge dynamic response data are normalized and divided into training set and verification set according to a predetermined proportion.

Step 2: Network optimization and training. An BiLSTM network with three-time sequence responses as input is constructed, and IPSO algorithm is used to optimize the network hyperparameters, in which the fitness value of each particle is the average value of all sample losses in the verification set. The optimized network is trained using the training set.

Step 3: Displacement response reconstruction. The network parameters are preserved once the network model is optimized and training is completed. The preprocessed input data is loaded into the trained IPSO-BiLSTM network to reconstruct the bridge displacement response.

Only a small number of sensors are required for the proposed method, which is meaningful in solving the problem that traditional dynamic displacement measurement is limited by installation difficulties. Besides, the proposed method effectively makes up for the shortcomings of the data fusion method based on neural network by constructing a triple-input IPSO-BiLSTM network with IPSO algorithm optimizing the network parameters.

4. Numerical study

Numerical study is conducted on a simply supported beam to investigate the performance of the proposed method. The finite element model (FEM) of vehicle-beam system is established to calculate the dynamic response of beam caused by moving vehicle load, and a dataset is constructed for IPSO-BiLSTM network.

The main parameters for the beam are as follows: beam length $L = 3\,m$, linear density $p = 8.75\,\mathrm{kg}/m$, elastic modulus $E = 70\,\mathrm{Gpa}$, and inertia moment $I = 1.4 \times 10^{-7}\,m^4$. The half vehicle model (Zacchei *et al*. 2023)

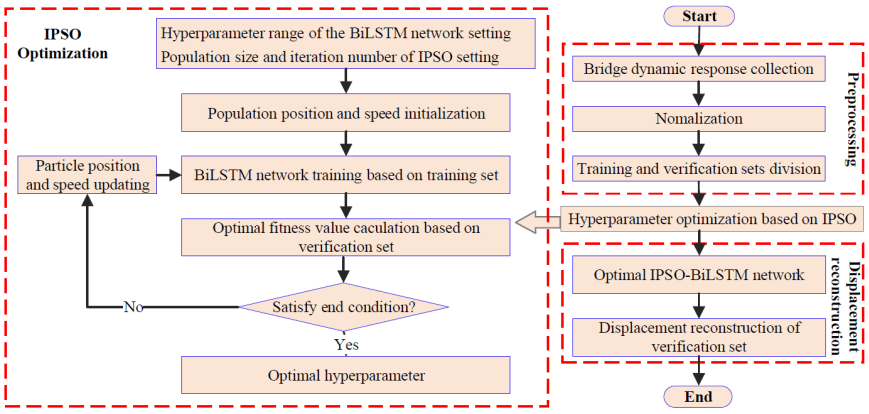

Fig. 3 Bridge dynamic displacement reconstruction procedure

(Fig. 4(a)) is adopted in this example. In Fig. 4(a), b_1 and b_2 represent the front and rear axle lengths, respectively; k_1 and k_2 represent the stiffness of the front and rear wheels, respectively; c_1 and c_2 represent front and rear wheel damping, respectively. The sensor arrangement is shown in Fig. 4(b). Two strain sensors are arranged at the $\frac{2}{5}$ span and $\frac{3}{5}$ span of the bridge, and one acceleration sensor and one displacement sensor are arranged at the mid-span of the beam. The simply supported beam is evenly divided into 20 beam elements, and the FEM of vehicle-bridge is established to calculate the strain, acceleration and displacement responses of the beam. The sampling frequency is set as 1000 Hz.

The triple-input BiLSTM network with three neurons in the hidden layer to be optimized is established. The strain response of two measuring points and the acceleration response at the mid-span are taken as input response, while the measured displacement response is used for reference. The vehicle weight is assumed to be 2 kg to 5 kg with step of 0.05 kg, while the vehicle velocity is assumed to be $0.2\,m/s$ to $1.5\,m/s$ with step of $0.01\,m/s$. The vehicle travels on the simply supported beam with different combinations of vehicle weight and velocity. The front and rear axle length, front and rear axle stiffness, and front and rear axle damping of the vehicle are randomly determined according to the interval in Table 1. A total of 7991 samples are established as the training set. The value range of strain and displacement data is normalized to [0, 1] by Eq. (12), and the value range of acceleration data is normalized to [-1, 1] by Eq. (13). For Case C-N in verification set, the vehicle weight and velocity are 1.9 kg and $1.6\,m/s$, respectively. IPSO is used to optimize the hyperparameters (number of hidden layers, number of neurons in the three hidden layers, training period, and learning rate) of the Bi-LSTM network. The range of the position and speed of the hyperparameter are listed in Table 2. The parameter initialization of IPSO is shown in Table 3. The normalized root mean square error (NRMSE) is defined to evaluate the reconstruction accuracy as (Eq. (14)).

$$NRMSE(\%) = 100\sqrt{\frac{\sum(u_p - u_l)^2}{\sum(u_l)^2}} \tag{14}$$

where u_l and u_p denote the reference and reconstructed displacement, respectively.

The optimization of hyperparameters is critical for balancing the capacity and generalization of network model. For instance, an insufficient number of neurons fails to capture high-frequency vibrations in strain data, while excessive neurons amplify noise interference. And insufficient neurons may result in the loss of pivotal features, while too many neurons increase the computational cost and introduce redundant parameters, reducing model robustness. Besides, too few training cycles can lead to model underfitting, while too many training cycles will lead to overfitting. Similarly, a high learning rate causes unstable convergence, whereas a low rate slows down the training process. The IPSO algorithm adaptively adjusts these parameters based on real-time fitness values, ensuring

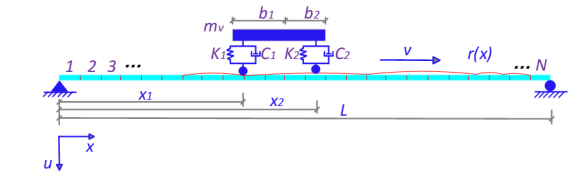

(a) One-half vehicle model

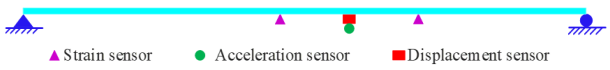

(b) Sensor arrangement

Fig. 4 Vehicle model and sensor arrangement

Table 1 Uncertainty in vehicle model

Vehicle parameters	Value interval
Front and rear axle length (m)	[0.079,0.081]
Front and rear axle stiffness (kN/m)	[5.2 × 104, 5.2 × 104]
Front and rear damping (N/m/s)	[30,35]

Table 2 Range of the hyperparameters

Hyper parameter	Position range	Velocity range
Number of hidden layers	[1, 3] (integer)	[-2, 2]
Number of neurons	[64,128] (integer)	[-20, 20]
Training cycle	[1, 8] (integer)	[-3, 3]
Learning rate	[0.00005, 0.00015]	[-0.0003, 0.0003]

Table 3 Parameter initialization of the IPSO

Parameter	Value
Population size	10
Inertia weight ω_{min}	0.4
Inertia weight ω_{max}	0.9
Maximum number of iterations	15

that the network maintains optimal performance under varying load and noise conditions.

Firstly, 50% of the training set samples are used for hyperparameter optimization. As shown in Fig. 5, the optimal fitness value tends to be stable and the optimal solution can be obtained after 8 iterations. The number of hidden layers in the optimal network is 2, and the optimal number of neurons corresponding to the three input responses is 112, 124 and 95, respectively. The optimal learning rate is 0.000087, and the optimal training period is 6. Then the optimal hyper-parameters are input to the triple-input IPSO-BiLSTM network, and the network model is trained by using the training set. Finally, the verification set samples are input into the trained network to output the dynamic displacement at mid-span, and the results are shown in Fig. 6. Table 4 compares the reconstruction accuracy of a dual-input IPSO-BiLSTM network with strain response at 2/5 span and 3/5 span as input and a dual-input IPSO-BiLSTM network with acceleration response at 2/5 span and 3/5 span as input. The reconstruction error of

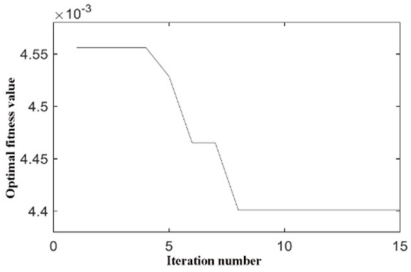

Fig. 5 Optimal fitness value in Case C-N

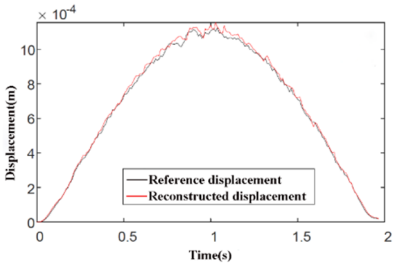

Fig. 6 Comparison of reconstructed and reference displacement of Case C-N

triple-input IPSO-BiLSTM network is 2.36%, which is 1.61% and 2.72% lower than that of dual-input IPSO-BiLSTM network based on strain only or acceleration only. It can be concluded that fusing acceleration and strain response can reduce the reconstruction error of moving vehicle load induced displacement.

5. Discussion

5.1 Road roughness

In "Vehicle vibration-describing method for road surface irregularity (GB/T7031-86)", the road surface is divided into 8 grades according to the power spectral density. The influence of road roughness on bridge dynamic displacement reconstruction accuracy is investigated by the simply supported beam in Section 3 with vehicle weight 1.9 kg and vehicle velocity 1.6 m/s. In this section, "Grade A" and "Grade B" road surface are simulated, and the road roughness coefficients are taken as 0, 8, 16, 32 and 64, respectively, which are deemed as Cases C-R-0, C-R-1, C-R-2, C-R-3 and C-R-4, respectively. The reconstructed displacement at mid-span is shown in Fig. 7, and the error indexes are listed in Table 5. The NRMSE is 3.57% when the road roughness coefficient is 8. However, the NRMSE increases to 7.05% when the road roughness coefficient is 32, which means that the road roughness significantly influences the reconstruction accuracy. The sensitivity to road roughness (Fig. 7) highlights a critical challenge: the performance of the network is bound by the diversity of training scenarios. For instance, the NRMSE escalates to 10.65% under Grade D roughness (Case C-R-4), where high-frequency vibrations exceed the effective bandwidth of strain sensors. Besides, the dynamic response is more complex for high road grades, therefore it is difficult to map the complex nonlinear relationship under different road roughness. Therefore, the current framework requires further improvement in handling untrained road conditions. Future work could integrate physics-informed constraints into the neural network to enhance extrapolation capability.

5.2 Measurement noise

In real bridge test, the measured signal inevitably contains noise due to the influence of sensor, acquisition system and environment. To explore the robustness of the proposed method, noise is added to the simulated signal according to Eq. (15)

$$u_z = u + E_p N_{noise} \times \sigma(u) \tag{15}$$

where u_z is the response signal with noise, E_p is the noise level, N_{noise} is the independent random variable vector obeying the standard normal distribution, and $\sigma(u)$ is the standard deviation of the response.

The simply supported beam in Section 3 is reused to examine the measurement effects. Four noise levels, specific as 0, 3%, 5% and 7% are added into the strain response and acceleration response, respectively, which are deemed as Cases C-N-1, C-N-2, C-N-3 and C-N-4, respectively, while other parameters remain unchanged. The displacement reconstruction results are shown in Fig. 8, and the error indexes are summarized in Table 6. The results manifested that the reconstruction error increases with the noise level. When the noise level is less than 5%, the NRMSE is within 5%, and when the noise level is 7%, the NRMSE increases to 7.38%.

The degradation under high noise levels reveals a critical trade-off between noise suppression and feature preservation. While the IPSO-BiLSTM network inherently mitigates noise through multi-source data fusion, its performance is constrained by the spectral characteristics of sensor signals. For instance, strain sensors' low-frequency dominance makes them vulnerable to baseline drift, whereas acceleration noise aliasing during integration amplifies high-frequency errors. To further enhance noise robustness, future work could integrate domain-specific denoising techniques. For example, wavelet-based filtering for strain signals and band-stop filtering for acceleration

Table 4 Comparison of reconstruction accuracy of different networks

Network model	NRMSE (%)
Triple-input IPSO-BiLSTM network	2.36
Dual-input IPSO-BiLSTM network (strain-based only)	3.97
Dual-input IPSO-BiLSTM network (acceleration-based only)	5.08

Table 5 Displacement reconstruction accuracy under different road grades

Case	Road roughness coefficient $(10^{-6}m^2/m^{-1})$	NRMSE (%)
Case C-R-0	0	2.36
Case C-R-1	8	3.57
Case C-R-2	16	5.55
Case C-R-3	32	7.08
Case C-R-4	64	10.65

Table 6 Displacement reconstruction accuracy at different noise levels

Cases	Noise level	NRMSE (%)
C-N-1	0%	1.54
C-N-2	3%	1.76
C-N-3	5%	4.78
C-N-4	7%	7.38

data may suppress noise without distorting the response patterns.

6. Experiment verification

A vehicle-beam model is established to verify the effectiveness of the proposed method in the laboratory environment. The experimental procedures are as follows:

(1) Experiment arrangement. The layout of the experimental model is shown in Fig. 9. Aluminum simply supported beams are selected as the main beam, and approach beams with a length of 1 m are set at both ends. The front-end approach beam is used for acceleration to ensure the trolley to reach a predetermined velocity, while the rear approach beam enables the trolley to slow down at enough distance after getting off the main beam. All beams are erected on triangular iron bearings. The parameters for the main bridge are: length 3 m, width 0.125 m, height 0.025 m, elastic modulus 70 Gpa, and density 2700 kg/m^3. The test trolley with a wheelbase of 0.16 m and a weight of 0.1 kg is shown in Fig. 10(a). Baffles are set on both sides of the beam to limit the straight movement of the trolley. A motor is used to tow the trolley in which the vehicle velocity is controlled by a frequency modulator. The sensors used in the experiment are shown in Fig. 10(b). One strain sensor is arranged on the lower surface of the beam at 2/5 span and 3/5 span of the main beam, and one displacement sensor and one acceleration sensor are arranged below the middle span of the beam. The top of the displacement sensor is placed at the lower part of the beam, and the strain sensor and acceleration sensor are adhered to the lower part and positioned on the central axis of the beam. The top of the displacement sensor is placed at the lower part of the beam, and the strain sensor and acceleration sensor are adhered to the lower part and positioned on the central axis of the beam.

(2) Training set establishment. The FEM of the experimental system is established to generate enough data for network training. The trolley mass is assumed to be 2 kg to 5 kg with step of 0.05 kg and the vehicle velocity is assumed to be 0.2 m/s to 1.5 m/s with step of 0.01 m/s. The trolley passes through the beam with different combinations of trolley weight and velocity. The front and rear axle length, front and rear axle stiffness and front and rear axle damping of the trolley are random

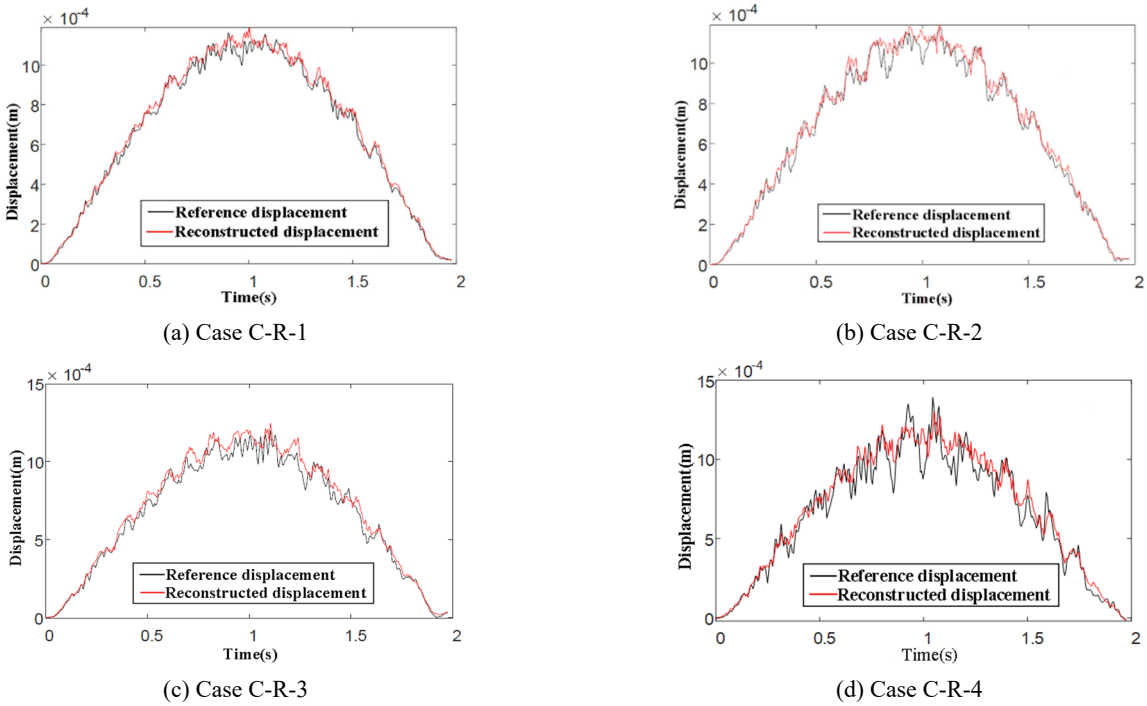

(a) Case C-R-1 (b) Case C-R-2

(c) Case C-R-3 (d) Case C-R-4

Fig. 7 Comparison of reconstructed and reference displacement under different road roughness

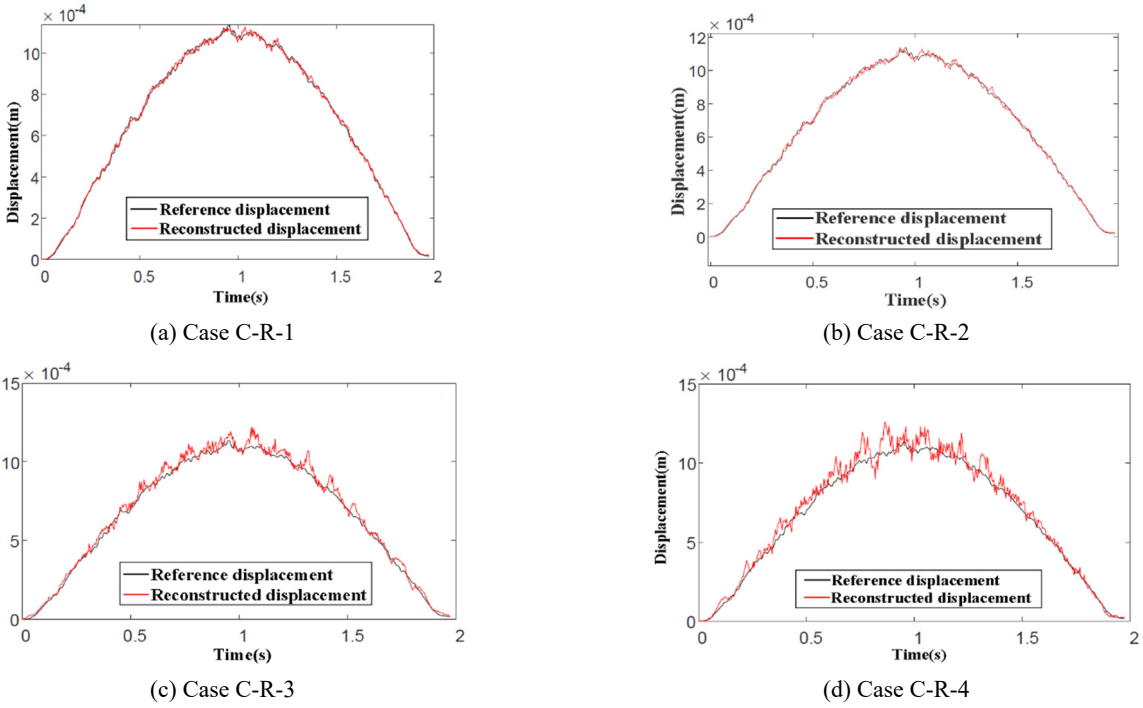

(a) Case C-R-1 (b) Case C-R-2

(c) Case C-R-3 (d) Case C-R-4

Fig. 8 Comparison of reconstructed and reference displacements with different noise level

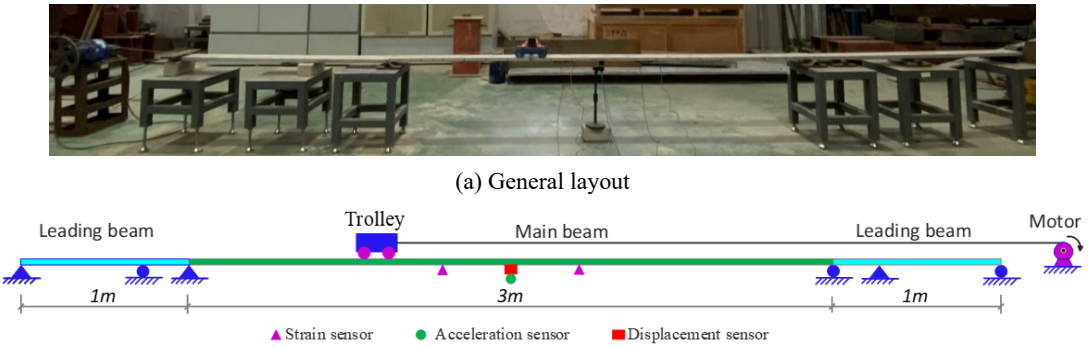

(a) General layout

(b) Sensor layout

Fig. 9 Experiment layout

(a) Test trolley (b) Sensor

Fig. 10 Experiment equipment

determined according to the intervals in Table 4. A total of 7991 samples are taken to calculate the beam response and establish training set.

(3) Hyperparameter optimization and network training. The triple-input IPSO-BiLSTM network is constructed firstly. Then, the value range of network hyperparameters is determined according to Table 1, and the parameters of the IPSO algorithm are initialized according to Table 2. 50% of the training set samples are used for network hyperparameter optimization. The optimization results manifest that the optimal fitness value tends to be stable after 11 iterations, and the optimal solution of hyperparameters can be obtained accordingly.

(4) Verification set establishment. The trolley with the weight of 1.5 kg is towed by the motor with the constant turning frequency of 3 Hz on the beam. The dynamic

Table 7 Influence of the vehicle velocity and weight

Factor	Case classification and reconstruction accuracy				
Trolley velocity	Motor rotation frequency	1 Hz	2 Hz	3 Hz	4 Hz
	Trolley weight 2 kg	C-V-1	C-V-2	C-V-3	C-V-4
	NRMSE (%)	4.56	4.41	4.62	5.32
Trolley weight	Trolley weight	1.5 kg	2.5 kg	3.5 kg	4.5 kg
	Motor rotation frequency	C-M-1	C-M-2	C-M-3	C-M-4
	NRMSE (%)	4.05	4.94	5.36	6.23

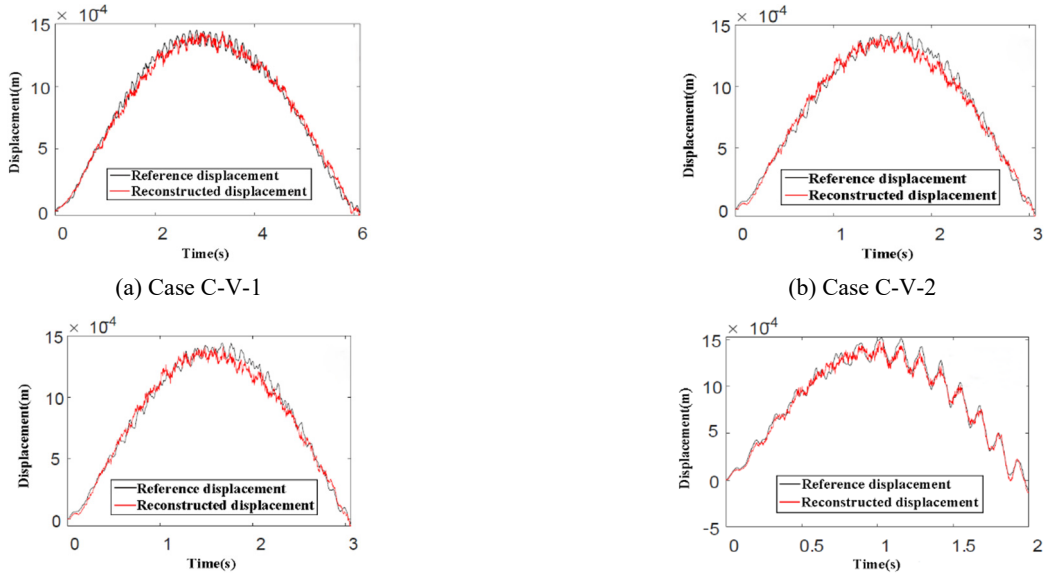

(a) Case C-V-1 (b) Case C-V-2

(c) Case C-V-3 (d) Case C-V-4

Fig. 12 Comparison of reconstructed and reference displacement in Case C-V-1 to Case C-V-4

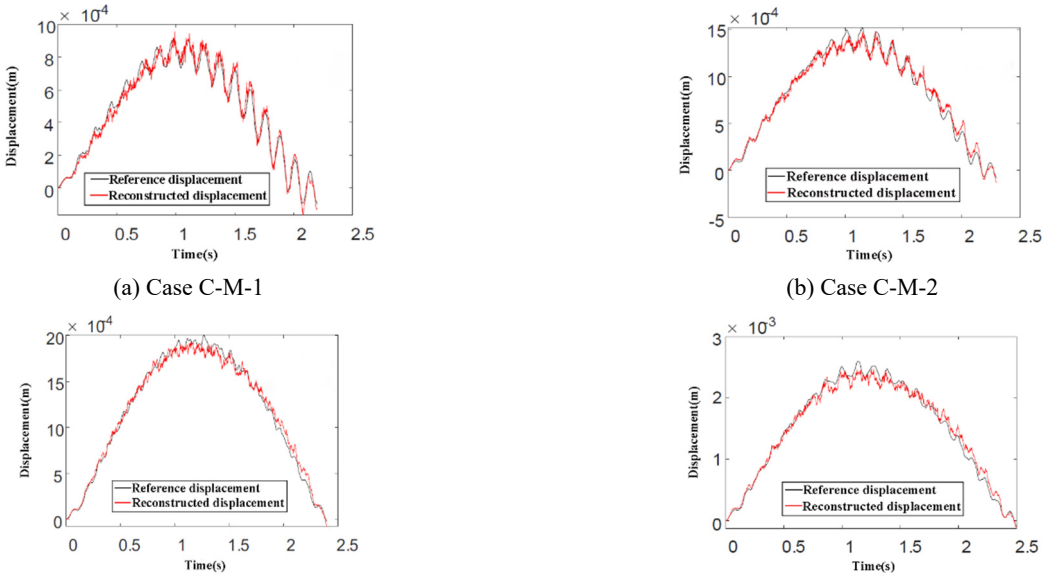

(a) Case C-M-1 (b) Case C-M-2

(c) Case C-M-3 (d) Case C-M-4

Fig. 13 Comparison of reconstructed and reference displacement in Case C-M-1 to Case C-M-4

responses of the measuring point are collected by a data acquisition instrument, and the sampling frequency is set to be 1000 Hz. The corresponding data is employed to establish the verification set, deemed as Case C-C-0.

(5) Dynamic displacement reconstruction. Two strain response sequences and one acceleration response sequence

collected in Step (4) are input into the trained network. The dynamic displacement at mid-span is reconstructed and shown in Fig. 11. Similar to the numerical study, the proposed method can effectively reconstruct the moving load induced displacement by in the experimental environment.

(6) Influence factor analysis. To examine the influence of trolley velocity and weight on the reconstruction accuracy, the trolley passes through the aluminum beam with different combinations of vehicle trolley and velocity (Table 7). When the trolley weight is 2 kg, the motor frequency is set to be 1 Hz to 4 Hz with step of 1 Hz, which are deemed as Cases C-V-1, C-V-2, C-V-3 and C-V-4, respectively. When the motor frequency is 3 Hz, the trolley weight is set to be 1.5 kg to 4.5 kg with step of 1 kg, which are deemed as Cases C-M-1, C-M-2, C-M-3 and C-M-4, respectively. The reconstruction results are presented in Figs. 12 and 13, and the error index NRMSEs are about 5% (Table 7). It can be concluded that the trolley weight and vehicle velocity have little influence on the reconstruction accuracy of the proposed method.

7. Conclusions

A reconstruction method for bridge displacement response induced by moving load was proposed by using a small number of sensors and IPSO-BiLSTM network. The effectiveness and superiority of the method were verified by numerical simulation and laboratory experiment, and the effects of road roughness, measurement noise, vehicle velocity and weight on the reconstruction accuracy were systematically investigated. The conclusions are as follows:

(1) The proposed triple-input IPSO-BiLSTM network realized the data fusion of three-time sequence responses and automatically established the relationship between input response and output displacement with the hyperparameters determined by IPSO algorithm.

(2) The proposed method used only a small number of sensors, which effectively relieved the problems of traditional dynamic displacement measurement limited by installation difficulties.

(3) The results of numerical examples indicated that the reconstruction accuracy was sensitive to road roughness and measurement noise. When the road roughness coefficient was less than 16 or the input signal noise level was less than 7%, the reconstruction displacement was basically consistent with the reference displacement. The experiment manifested that the reconstruction accuracy was insensitive to vehicle velocity and vehicle weight, and the displacement reconstruction error under different load conditions are no more than 6.23%.

The transition from laboratory validation to real-world deployment necessitates addressing scalability, sensor durability, and environmental adaptability. For instance, while the proposed method reduces sensor deployment costs, its reliance on low-cost sensors introduces bandwidth limitations that may miss critical high-frequency vibrations in complex bridges. Future work should explore hybrid sensing systems combining fixed low-cost sensors with mobile high-precision equipment (e.g., UAV-mounted LiDAR) to balance cost and accuracy. Besides, environmental robustness can be enhanced through hardware innovations (e.g., hermetic sensor packaging) and algorithmic adaptations (e.g., temperature-invariant feature extraction).

Acknowledgments

The paper is supported by National Natural Science Foundation of China (52378298), Natural Science Fund for Distinguished Young Scholars of Anhui Province (2208085J20), and Fundamental Research Funds for the Central Universities (PA2024GDGP0036).

References

Cheng, Y.Y., Zhang, L., Jiang, M.S. and Sui, Q.M. (2018), "Strain/Displacement field reconstruction and load identification of high-speed train load-bearing structure based on linear superposition method", *IEEE T. Instrum. Meas.*, **71**, p. 7003408. https://doi.org/10.1109/TIM.2022.3169529

Ehsan, F., Saeed, F., Kowsar, N. and Jens, P.C. (2022), "Analyzing GNSS measurements to detect and predict bridge movements using the Kalman filter (KF) and neural network (NN) techniques", *Geomatics*, **1**(1), 65-80. https://doi.org/10.3390/ geomatics1010006

Gad, A.G. (2022), "Particle swarm optimization algorithm and its applications: a systematic review", *Arch. Comput. Method Eng.*, **29**(5), 2531-2561. https:// doi.org/10.1007/s11831-021-09694-4

Guan, S.Y., Rice, J.A., Li, C.Z., Li, Y.R. and Wang, G.C. (2015), "Dynamic and static structural displacement measurement using backscattering DC coupled radar", *Smart Struct. Syst., Int. J.*, **16**(3), 521-535. https://doi.org/10.12989/sss.2015.16.3.521

Hassani, S., Dackermann, U., Mousavi, M. and Li, J.C. (2023), "A systematic review of data fusion techniques for optimized structural health monitoring", *Inform. Fusion*, **103**, p. 102136. https://doi.org/10.1016/j.inffus.2023.102136.

Hester, D., Brownjohn, J., Bocian, M. and Xu, Y. (2017), "Low cost bridge load test: Calculating bridge displacement from acceleration for load assessment calculations", *Eng. Struct.*, **143**, 358-374. https://doi.org/10.1016/j.engstruct.2017.04.021

Joshi, S. and Harle, S.M. (2017), "Linear variable differential transducer (LVDT) & its applications in civil engineering", *Int. J. Transp. Sci. Tech.*, **3**(4), 62-66. https://doi.org/10.11648/j.ijtet.20170304.13

Kim, K. and Sohn, H. (2017), "Dynamic displacement estimation by fusing LDV and LiDAR measurements via smoothing based Kalman filtering", *Mech. Syst. Signal Pr.*, **82**, 339-355. https://doi.org/10.1016/j.ymssp.2016.05.027

Kogan, M.G., Kim, W.Y., Bock, Y. and Smyth, A.W. (2008), "Load response on a large suspension bridge during the NYC Marathon revealed by GPS and accelerometers", *Seismol. Res. Lett.*, **79**(1), 12-19. https://doi.org/10.1785/gssrl.79.1.12

Kumar, G., Singh, U.P. and Jain, S. (2022), "An adaptive particle swarm optimization-based hybrid long short-term memory model for stock price time series forecasting", *Soft Comput.*, **26**, 12115-12135. https://doi.org/10.1007/s00500-022-07451-8

Lee, H.S., Hong, Y.H. and Park, H.W. (2010), "Design of an FIR filter for the displacement reconstruction using measured acceleration in low-frequency dominant structures", *Int. J. Numer. Meth. Eng.*, **82**(4), 403-434. https://doi.org/10.1002/nme.2769

Ma, Z., Chung, J., Liu, P. and Sohn, H. (2021), "Bridge

displacement estimation by fusing accelerometer and strain gauge measurements", *Struct. Control Health Monitor.*, **28**(6), p. e2733. https://doi.org/10.1002/stc.2733

Martini, A., Tronci, E.M., Feng, M.Q. and Leung, R.Y. (2022), "A computer vision-based method for bridge model updating using displacement influence lines", *Eng. Struct.*, **259**, p. 114129. https://doi.org/10.1016/j.engstruct.2022.114129

Moon, H.S., Ok, S., Chun, P.J. and Lim, Y.M. (2019), "Artificial Neural Network for Vertical Displacement Prediction of a Bridge from Strains (Part 1): Girder Bridge under Moving Vehicles", *Appl. Sci.*, **9**(14), p. 2881. https://doi.org/10.3390/app9142881

Moreu, F., Jo, H., Li, J., Kim, R.E., Cho, S., Kimmle, A., Scola, S., Le, H., Spencer, B.F. and LaFave, J.M. (2015), "Dynamic assessment of timber railroad bridges using displacements", J. *Bridge Eng.*, **20**(10), p. 04014114. https://doi.org/10.1061/(ASCE) BE.1943-5592.0000726

Nakamura, S. (2000), "GPS measurement of wind-induced suspension bridge girder displacements", *J. Struct. Eng.*, **126**(12), 1413-1419. https://doi.org/10.1061/(ASCE)07339445 (2000)126:12(1413)

Nassif, H.H., Gindy, M. and Davis, J. (2005), "Comparison of laser Doppler vibrometer with contact sensors for monitoring bridge deflection and vibration", *Ndt & E Int.*, **38**(3), 213-218. https://doi.org/10.1016/j.ndteint.2004.06.012

Ni, Y.Q., Wang, Y.W., Liao, W.Y. and Chen, W.H. (2019), "A vision-based system for long-distance remote monitoring of dynamic displacement: experimental verification on a supertall structure", *Smart Struct. Syst.*, *Int. J.*, **24**(6), 769-781. https://doi.org/10.12989/sss.2019.24.6.769

Nickabadi, A., Ebadzadeh, M.M. and Safabakhsh, R. (2011), "A novel particle swarm optimization algorithm with adaptive inertia weight", *Appl. Soft Comput.*, **11**(4), 3658-3670. https://doi.org/10.1016/j.asoc.2011.01.037

Park, J.W., Sim, S.H. and Jung, H.J. (2013), "Displacement estimation using multimetric data fusion", *IEEE-ASME T. Mech.*, **18**(6), 1675-1682. https://doi.org/10.1109/TMECH.2013.2275187

Ruhm, K.H. (2007), "Sensor fusion and data fusion – mapping and reconstruction", *Measurement*, **40**(2), 145-157. https://doi.org/10.1016/j.measurement.2006.07.012

Shin, S., Lee, S.U., Kim, Y. and Kim, N.S. (2012), "Estimation of bridge displacement responses using FBG sensors and theoretical mode shapes", *Struct. Eng. Mech., Int. J.*, **42**(2), 229-245. https://doi.org/10.12989/sem.2012.42.2.229

Smyth, A. and Wu, M.L. (2007), "Multi-rate Kalman filtering for the data fusion of displacement and acceleration response measurements in dynamic system monitoring", *Mech. Syst. Signal Pr.*, **21**(2), 706-723. https://doi.org/10.1016/j.ymssp.2006.03.005

Stiros, S.C. (2008), "Errors in velocities and displacements deduced from accelerographs: An approach based on the theory of error propagation", *Soil Dyn. Earthq. Eng.*, **28**(5), 415-420. https://doi.org/10.1016/j.soildyn.2007.07.004

Vurpillot, S., Krueger, G., Benouaich, D., Clement, D. and Lnaudi, D. (1998), "Vertical deflection of a pre-stressed concrete bridge obtained using deformation sensors and inclinometer", *ACI Struct. J.*, **95**, 518-526.

Wang, Z.C., Geng, D., Ren, W.X. and Liu H.T. (2014), "Strain modes based dynamic displacement estimation of beam structures with strain sensors", *Smart Mater. Struct.*, **23**(12), p. 125045. https://doi.org/10.1088/0964-1726/23/12/125045

Wang, Z.C., Duan, D.Y., Sun, X.T. and Xin, Y. (2022), "A data fusion method for bridge displacement reconstruction based on LSTM networks", *Smart Struct. Syst.*, *Int. J.*, **29**(4), 599-616. https://doi.org/10.12989/sss.2022.29.4.599

Zacchei, E., Lyra, P.H.C., Lage, G.E., Antonine, E., Soares Jr., A.B., Caruso, N.C. and Assis, C.S. (2023), "Structural health monitoring and mathematical modelling of a site-specific concrete bridge under moving two-axle vehicles", *Int. J. Civil Eng.*, **21**, 427-443. https://doi.org/10.1007/s40999-022-00770-9